UNIVERSIDAD DE CÓRDOBA

Facultad de Ciencias

Grado de Física

Trabajo Fin de Grado

Luminescent response study of ionic crystals used in dosimetry

Código del TFG: **FS24-008-FSC**

Tipo de TFG: **Trabajo de iniciación a la investigación**

Autor: Marta de la Rosa Núñez

Fecha de entrega

Agradecimientos

Incluir los agradecimientos, si procede.

Índice general

Índice de figuras

Índice de tablas

Resumen

Escriba aquí un resumen de la memoria en castellano que contenga entre 100 y 300 palabras. Las palabras clave serán entre 3 y 6.

Palabras clave: palabra clave 1; palabra clave 2; palabra clave 3; palabra clave 4

Abstract

Insert here the abstract of the report with an extension between 100 and 300 words.

Keywords: keyword1; keyword2; keyword3; keyword4

CAPÍTULO 1

Introduction

As a bystander, one may pass life without thinking of the things that surrounds us. One may have had the misfortune of entering on an MRI, or the responsability to carry a dosimeter in a nuclear plant, and stepped out the room as it is. Life can go on unquestioned, and one may get out of that PET scan without thinking of the source of that awful noise.

There's beauty in the mundane, and the world is full of wonders. The universe is a complex system of interactions, and we know a very small part of it. We are surrounded by radiation, and we are constantly exposed to it. It is a natural phenomenon that has been present since the beginning of time, and it is an integral part of our existence. There are answers for those who wonder, and this work is a very small step towards it.

Luminescence is a phenomenon familiar to us; and goes through our lives like a commercial break. We see it in the glow of a firefly, the sparkle of a diamond, or the light emitted by a fluorescent lamp. In a nutshell, it is a process where energy is absorbed and re-emitted as light, leaving a trail behind, and can be triggered by various stimuli, like heat, light or radiation. This broad notion is the reason why the study of luminescence has practical uses in many fields. One of those fields of use is the detection of ionizing radiation, a field generally known as "dosimetry". The amount of radiation absorbed by a material can be measured by the amount of light emitted when the material is stimulated, and this is the basis for many dosimetry techniques. These luminescence-based methods for detecting ionizing radiation have played a central role in radiation research since the earliest discoveries of radiation, as they exploit the ability of specific materials to emit light when exposed to ionizing radiation, to detect and quantify the radiation received, further expanding the knowledge its efect.

One of the most commonly used materials in this context is lithium fluoride doped with magnesium and titanium (LiF:Mg,Ti). This material exhibits thermoluminescence, a phenomenon where after irradiation, its internal structure captures a memory of the event, in the form of trapped electrons. Upon heating, these trapped charges are released; recombining and emitting photons in the process. The resulting light —that we know to be called luminescence—, if recorded as a function of temperature, produces what is called a thermoluminescence (TL) glow curve.

But knowing that LiF:Mg, Ti emits light when heated is only the beginning. The real challenge lies in understanding it. Interpreting it. The glow curve, with its peaks and valleys, is more than a passive result. It is a message from within the material, shaped by the dance of the electrons accross the imperfections of the lattice, and it tells a story —if we know how to read it.

To make sense of that story, one must model it. That is, to simulate the physical processes that give rise to the observed glow, and to see whether our mathematical model truly mirror nature. Can we, with a set of parameters and approximations, recreate the fingerprint of radiation? Can we extract from that curve a clear image of the processes within?

This is where this work begins. At the heart of this discourse lies the attempt to reproduce the TL glow curve of LiF:Mg, Ti through computational modeling. This effort leans on the shoulders of many brilliant scientists with an insatiable hunger for one of the many misteries of the universe, one where electrons takes us across energy barriers, where recombination is probabilistic, and where heat becomes the catalyst of understanding.

But even the best models are incomplete. Many assume constant parameters —fixed frequency factors and activation energies, unchanged by temperature or entropy. Reality, as often, lies in a space in between. In these pages, it will be investigated what happens when we let these parameters breathe. By introducing temperature-dependent frequency factors, we will investigate how this modification reshapes the predicted glow curve. Is the model improved? Do we get closer to the experimental results? Can it go beyond known data and predict a hypothetical future case?

Ultimately, the motivation is simple: to understand. To refine our lens on thermoluminescence; to bridge the gap between theory and experience, and to contribute, even in the smallest way, to the slow unraveling of the invisible questions that shape our everyday lives.

CAPÍTULO 2

Objectives

CAPÍTULO 3

Theoretical framework

3.1. The mathematical model

To describe the thermoluminescent response of a semicoductor, we can use a mathematical model based on the trapping and releasing of charge carriers in the accesible energy levels of the material.

Let us first consider the case of an arbitrary semicoductor without impurities. The energy levels of the conduction band and the valence band are separated by a bandgap E_g, and can be obtained with Schrodinger's equation that is under the influence of a periodic potential:

$$\left[-\frac{\hbar^2}{2m}\nabla^2 + V(\vec{r})\right]\psi(\vec{r}) = E\ \psi(\vec{r}), \tag{3.1}$$

The periodicity of the potential $V(\vec{r})$ for any lattice vector $\vec{R}$ allows the Bloch's theorem to apply, and so it gives rise to the formation of a band structure, composed by the conduction band, which is typically fully occupied at absolute zero temperature, and the valence band, which is in turn typically empty -or rather, we can consider it filled with holes (h^+), or "positively charged electrons". The bandgap E_g is then defined as the energy difference between the top of the valence band and the bottom of the conduction band, and for a perfect crystal, no energy states are allowed in that region. This can be clearly seen if we take into account the density of available states, $D(E)$, which is a function of the Fermi-Dirac distribution $f(E)$ for a certain temperature T. This function gives the occupancy of any energy level E, and can be expressed as:

$$f(E) = \frac{1}{e^{\frac{E-E_f}{k_B T}} + 1}, \tag{3.2}$$

Where E_f is the Fermi Level, and k_B is the Boltzmann constant. If the system is in equilibrium, and we set the case of $T = 0K$, the occupancy function $f(E)$ will be equal

to 1 for all energy levels below the Fermi level, and 0 for all energy levels above it. This means that the occupancy function will be a step function, with a discontinuity at the Fermi level, and so we can see that there are no available states in the bandgap region.

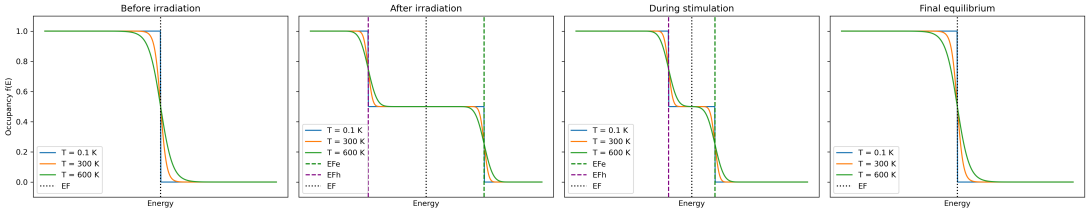

Figura 3.1: *Fermi-Dirac distribution for a semicoductor that is irradiated.*

The introduction of impurities or defects however, break the periodicity of the lattice, and create localized energy levels inside this "forbidden region". These levels can be thought of as traps for electrons if we are situated above the fermi level, and traps of holes if we are situated below. When this material is irradiated, electrons from the valence band can be excited to the conduction band, creating an electron-hole pair; and so changing the shape of the occupancy function. Once excited, both electrons and holes get "trapped" in these localized energy levels, and the excitation of these pairs into equilibrium will result in the emission of energy. In Figure 3.1 we can see a broad description of the perturbation of the system from its equilibrium state due to the irradiation, and the return of the system to equilibrium during either thermal stimulation or optical stimulation. If said relaxation processes are radiative, TL and OSL result.

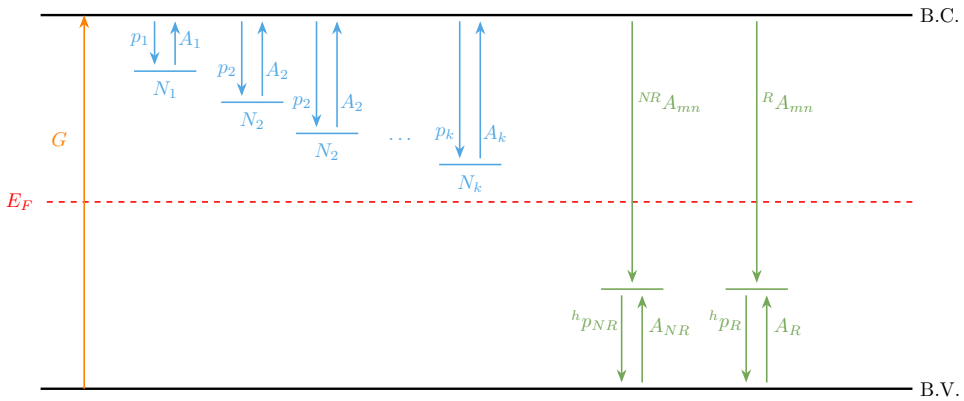

Figura 3.2: *Schematic representation of the theoretical model.*

And so, we can see a schematic representation of our theoretical model in Figure 3.2. Situating the energy in the Y axis, the focus is set in the energy gap of our material. Drawn as a blue or green horizontal line are the energy traps; in blue above the Fermi level there are electron traps, and in green there are hole traps or recombination centers. The vertical arrows describe available transitions; the ones pointing upwards represent an excitation process, and the ones pointing downwards represent a relaxation process.

Mathematically, we can describe these processes with a set of differential equations that take into account the rate of change of the number of electrons and holes in the bands and traps. This set will depend on the properties of the material, and the luminescence response we are trying to model. For an arbitrary system, we can write the following set of equations that describe the rate of change of the number of electrons and holes in the conduction band n_c, the valence band n_v:

$$\frac{dn_c}{dt} = G - \left[\sum_i \frac{dn_i}{dt}\right] \cdot n_c - \left[\sum_{j=R,NR} {}^{i}A_{mn} \cdot m_j\right] \cdot n_c \tag{3.3}$$

$$\frac{dn_i}{dt} = -p_i \cdot n_i + A_i \cdot [N_i - n_i] \tag{3.4}$$

$$\frac{dm_j}{dt} = -{}^{h}p_j \cdot m_j + A_j \cdot [M_j - m_j] \cdot n_v - {}^{i}A_{mn} \cdot m_j \cdot n_c \tag{3.5}$$

$$\frac{dn_v}{dt} = G - \sum_{j=R,NR} \left[-{}^{h}p_j \cdot m_j + A_j \cdot [M_j - mj] \cdot n_v\right] \tag{3.6}$$

Where every term is defined as follows:

- G: electron-hole pairs generated by the radiation [cm^{-3} s^{-1}]
- n_c: electron concentration in the conduction band [cm^{-3}]
- n_v: electron concentration in the valence band [cm^{-3}]
- n_i: electron concentration in trap i [cm^{-3}]
- m_j: hole concentration in the recombination center j [cm^{-3}]
- N_i: total density of electron trapping centres in trap i [cm^{-3}]
- M_j: total density of recombination centers [cm^{-3}]
- p_i: electron release probability factor for trap i [s^{-1}]
- ${}^{h}p_j$: hole release probability factor for recombination center j [s^{-1}]
- A_i: electron trapping probability factor for trap i [cm^3 s^{-1}]
- ${}^{i}A_{mn}$: recombination probability factor for recombination center j [cm^3 s^{-1}]

Equation 3.3 describes the change rate of electron concentrations in the conduction band. To interpret this equation, we can see that to the electron-hole pairs generated by the radiation (G), there are two terms substracted. The first one correlates to the electrons that leave the continuum levels of the conduction band and get trapped in the discrete levels of the material —a process described by 3.4, that will have a further discussion in section 3.2—, and the second one answers to the electrons in the conduction band that recombine with holes with a radiative (R) or non-radiative (NR) process. It is easy to see that this second term corresponds to the third term of 3.5.

The change rate of electron concentrations in the valence band is shown in 3.6, and it follows a similar logic. This time however, we only take into account the terms multiplied by the electron density in the valence band (n_v) seen in equation 3.5; one that represents the holes leaving the continuum to get trapped in the recombination centers, and another that accounts for the addition of electrons that are released from the recombination centers and recombine with the holes in the valence band. The terms described correspond to Equations 3.4 and 3.5 describe the total change rate of electrons and holes in the discrete levels of the material. The signs of the terms in these equations follow the convention that we are set in the conduction band, and so any electron that leaves the conduction band

is represented with a negative term, and any electron that enters is represented with a positive term.

To carry out a numerical simulation of the process, we will need to solve the set of differential equations 3.3 – 3.6 using RKF-45 method, which is a Runge-Kutta method of order 4 and 5. This method will obtain the charge concentration in all traps and recombination centers at an instant of time. The solving of this set of equations will be done for the three phases required to obtain the TL glow curve. To do this, the intrinsic and kinetic parameters are kept constant, varying the external conditions of the system such as temperature and electron-hole pair generation rate.

The first phase is *irradiation*, where the material is exposed to ionizing radiation. It begins with all levels initially empty $[n_c(0) = n_v(0) = n_i(0) = m_j(0) = 0]$, and the electron-hole pairs generated as a result will have a constant value as a function of time ($G = 1000$ cm^{-3} s^{-1}). The temperature is set to a constant $T = 25$ °C and the filling process takes one hour (3600 seconds). The second phase is *relaxation*, where the material is left undisturbed at a constant temperature for a defined period of time. Taking as initial values the final values of the irradiation phase, the temperature is kept constant at $T = 25$ °C, and the electron-hole pairs generation rate is set to $G = 0$ cm^{-3} s^{-1}. The relaxation process is set for one week (604,800 seconds). Finally, the third phase is *heating*, where the material is taken from an initial temperature T_0 to a final temperature at a constant linear heating rate during 400 seconds. The numerical resolution of the set equations is similar to the previous phases, but now with the temperature varying linearly with the expression:

$$T(t) = T_0 + \beta \cdot t \tag{3.7}$$

Where the heating rate is set to $\beta = 1$ °C s^{-1}. The electron-hole pairs generation rate is set to $G = 0$ cm^{-3} s^{-1}, and the charge concentration values are taken from the final values of the relaxation phase. The heating process is set to last 400 seconds. The results after the numerical resolution of the set of equations will be the charge concentration values for every instant of time throughout the whole heating cycle $[n_c(t), n_v(t), n_i(t), m_j(t)]$. It is in this phase when the luminescent emission occurs, and so the intensity of the emmited light can be estimated in relation to the radiative recombination of electron-hole pairs. We can give the expression for the intensity of the emitted light as it follows:

$$I(t) = -\frac{dm}{dt} \approx {}^{R}A_{mn} \cdot m_R \cdot n_c \tag{3.8}$$

Representing this intensity as a function of time will be the objective of the simulations, as it is the key to understand the thermoluminescent response of the $LiF : Mg, Ti$ after being irradiated.

3.2. The frequency factor

As introduced in Section 3.1, there is a greater discussion to be had about the releasing probability of electrons and holes, as it determines in great part the electron-hole pairs available to recombine. If we consider that after being irradiated, the material will release

its carriers through *thermal excitation*, an electron trapped in a lattice defect with energy E_t and temperature T will have a probability of being released that follows Arrhenius equation. The probability per second that the electron will be thermally excited into the conduction band is given by:

$$p = s \cdot e^{-\frac{E_t}{k_B T}} \tag{3.9}$$

Where s is known as the *frequency factor*. It can be interpreted as the "attempt to escape" frequency, as it is a measure of the number of times per second that energy is absorbed from phonons in the lattice. The exponential that follows is the probability that the energy absorbed is enough to cause a transition from the localized state to the conduction band.

The frequency factor is a very important parameter in the study of thermoluminescence, as it determines the rate at which electrons are released from traps. It is a function of the material properties, as shown in its definition:

$$s = \nu_{ph} \cdot K \cdot e^{\frac{\Delta S}{k_B}} \tag{3.10}$$

Where ν_{ph} is the lattice phonon vibration frequency and K is the transition probability constant. Typically, one can expect $s \sim 10^{12} - 10^{14}$ s^{-1}, which is consistent with the values of ν for most solids. The term $e^{\Delta S/k_B}$ is a correction factor that accounts for the entropy change associated with the transition from the localized state to the conduction band.

From equation 3.10 we see that the frequency factor has an exponential dependency with the entropy change. This, taking the Quantum Statistical Mechanics theory [3], does not align with the invariance of said factor with temperature, as entropy, with its own definition, should vary when temperature does. While a rigorous proof of the overall temperature dependence of the frequency factor is beyond the scope of this work, one model is proposed to provide an approximate perspective on how this dependency could influence the resulting TL glow curve.

At first glance, the simplest model was considered, where the entropy would be linear with the temperature ($\Delta S \propto T$). This theory was quickly discarded as would make the entropy factor increase exponentially with the temperature ($s \propto e^T$), and so the probability of excitation would tend to infinity in a very short range of temperature increase.

To solve this issue, a more refined model was considered, where the entropy would now be logarithmically dependent on the temperature ($\Delta S \propto \ln(T)$). The constant of the proportionality could be called α, and so the resulting expression of the frequency factor can be written as:

$$s = \nu_{ph} \cdot K \cdot T^{\alpha/k_B} \tag{3.11}$$

It is clear now that a softer dependency with the temperature is achieved, and the previous problem of the entropy factor tending to infinity is solved. The value of α can be adjusted to keep the entropy contribution at a realistic magnitude —typically we have $\Delta S \sim 1$–$3\ \ k_B$ over the glow curve temperature range—. For that reason, we have selected a value of:

$$\alpha = \frac{1.5\ k_B}{ln(300)} \approx 0.26\ k_B \tag{3.12}$$

This choice ensures that the frequency factor remains within a reasonable range across the temperature spectrum of interest, and yields TL glow curves that are consistent with experimental observations of LiF:Mg,Ti materials.

3.3. About LiF:Mg,Ti

Lithium fluoride (LiF) is a crystalline material that has been widely used in radiation dosimetry due to its favorable properties. It first appeared as a thermoluminescent dosimetry material in the 1950's, and since then, it has been extensively studied in the field of radiation detection. The material is composed of lithium (Li) and fluor (F) atoms, forming a crystal lattice structure of a face-centered cubic (FCC) type. Without any impurities, LiF is a semiconductor, with a bandgap of approximately 14 eV, which makes it an excellent insulator at room temperature.

To enhance the properties for radiation detection, LiF is often doped with magnesium (Mg) and titanium (Ti) ions, and sold commercially as TLD-100 [1]. The doping process introduces defects in the crystal lattice, creating energy levels within the bandgap. These defects play a crucial role in trapping and releasing charge carriers, which are responsible for the thermoluminescent response of the material. This process is known as thermoluminescence (TL), where the trapped electrons are released upon heating, resulting in the emission of light. The intensity of this emitted light is proportional to the amount of radiation absorbed by the material, making it a valuable tool for dosimetry.

The TL response of LiF:Mg,Ti is characterized by a glow curve, which is a plot of the intensity of emitted light as a function of temperature. The glow curve typically exhibits several peaks, each corresponding to different trapping levels in the material. The position and shape of these peaks can provide valuable information about the trapping and recombination processes occurring in the material, and they are key to understanding the thermoluminescent response of LiF:Mg,Ti.

CAPÍTULO 4

Simulations

4.1. Materials used for simulations

The materials used for this work are all the digital tools required for the simulation of the behaviour of our material of choice. In our case, the project was made using *Python* in a Jupyter Notebook. The programs written are available on the GitHub repository called `TFG_MartadelaRosa`.

The libraries used for the simulations are:

- `numpy`: This library is used for numerical calculations and array manipulations.
- `matplotlib`: This library is used for plotting graphs and visualizing data.
- `pandas`: This library is used for data manipulation and analysis, providing data structures like DataFrames.
- `scipy`: This library is used for scientific computing and includes functions for optimization, integration, interpolation, and more. In particular to solve the differential equations that describe the kinetics of the TL process.

4.2. Simulations

To compute a simulation of the TL process described in Section 3.1, after defining the parameters of the model, we need to solve the differential equations that describe the kinetics of the TL process. The equations are solved using the `odeint` function from the `scipy.integrate` library, which is a powerful tool for solving ordinary differential equations. The function takes as input the system of equations, the initial conditions, and the time points at which we want to evaluate the solution. The output is an array containing the values of the variables at each time point, which is then saved to their corresponding

variables, used to plot the results. They are brought to life using the `matplotlib` library, and for every resolution of the differential equations, we will present three graphs as the result.

CAPÍTULO 5

Results

5.1. Irradiation

After explaining the theoretical background of the problem and introducing the approach behind the simulations, we can now present the results obtained for the model we have developed. The results will always come in pairs, as we have done the same simulations for both the original model, where the frequency factor stays in a constant value (which we will call temperature independent), and the one we propose, where the frequency factor is a function of the temperature following equation 3.11 (temperature dependent). For this first section, we will focus on the graphs obtained from the simulations of the *irradiation* stage of the material. These can be seen in Figures 5.1– 5.3

First and foremost, we can start our analysis of the irradiation stage by looking at the evolution of the occupancy of the traps n_i as a function of time. In Figure 5.1 it is shown that the most prominent difference between the two models lies in what occurs with the trap I, shown by the blue line of n_I. In the temperature independent model, we see that all traps behave in a very similar way; they get gradually filled over time, as the electron-hole pairs are generated. There is a perceptible downward curve in the end of the irradiation time for the n_I trap, which could hint that the trap is being filled to its maximum capacity, but it is not very clear. In the temperature dependent model however, we see that the filling of the n_I trap is much more noticeable, and in turn the growth of the rest of the traps is more pronounced. We see that, whithout a doubt, the trap I is saturated in the first few minutes of irradiation.

If we look at recombination rates, in Figure 5.2 we can see that both models show a very similar behavior, with the exception of the steep of growth of the radiative recombination rate. In the temperature independent model, the growth is slowed compared to the temperature dependent model, indicating a higher trap occupation. Overall, it is a similar behavior than the one seen in 5.1, as it can be explained with the same principle. When making the frequency factor dependent of temperature, thermal energy dynamics are added, which facilitates the excitation and mobility of our charged carriers. This leads to a higher occupation of traps —beginning with the one closer to the Fermi level, trap

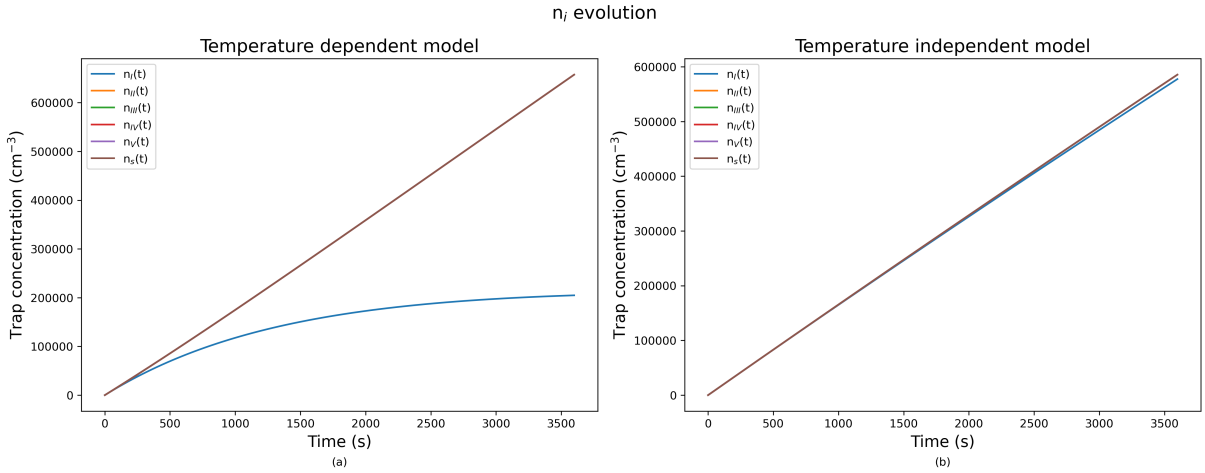

Figura 5.1: *Evolution of trap concentrations $n_i(t)$ plotted against time for the LiF:Mg, Ti during the irradiation phase for both models (a) Temperature dependent model, where the probabilities of excitation vary with temperature; (b) Temperature independent model, where the excitation probabilities are fixed parameters. Both were subjected to a constant irradiation rate of $G = 1000\ cm^{-3}\ s^{-1}$ and a laboratory temperature of $T = 25\ ^{\circ}C$ during 3600 seconds. The traps are labeled as follows: I (blue), II (orange), III (green), IV (red), V (purple), and s (brown).*

I—, which mathematically translates to higher slope in the graphs. Also, the nearly flat and negligible $dm_{NR}(t)$ in both cases suggests that non-radiative processes play a minimal role under these conditions.

The last graph to analyze is the one introduced in Section 4.2 to validate the model. In Figure 5.3 we can see that both models satisfy the charge neutrality condition, as the (cual es la condición????)

5.2. Relaxation

After the irradiation stage, we can now analyze the results obtained from the *relaxation* stage of the material. The graphs obtained from the simulations can be seen in Figures 5.4–5.6.

Again, the graphs will be presented in pairs, one for the temperature independent model and one for the temperature dependent model. The first graph to analyze is the evolution of the occupancy of the traps n_i as a function of time, which can be seen in Figure 5.4. At a first glance, one can clearly see a difference between the two figures, divided by one main factor: how does the detrapping work. By keeping the laboratory temperature at a fixed value, the probability of thermal detrapping is constant over time, and without electron-hole pair generation, the system evolves solely thorugh the release of previously trapped carriers. As a result, the relaxation dynamics are governed by the intrisic properties of each trap —specifically the activation energy and frequency factor—, which determine how trapped carriers will evolve.

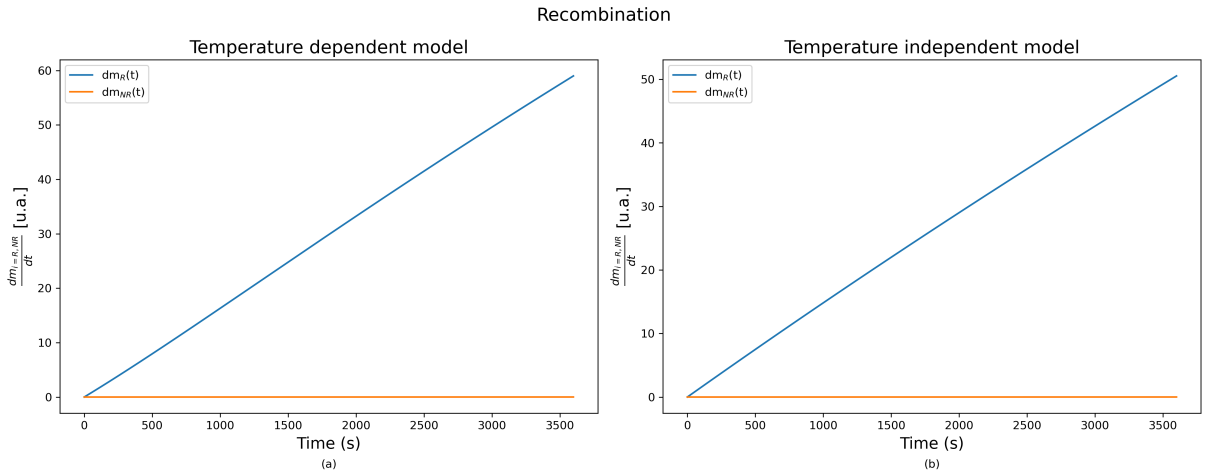

Figura 5.2: *Recombination rates during the irradiation phase for both models. (a) Temperature-dependent model; (b) Temperature-independent model. The plotted quantities correspond to the radiative (dm_R/dt) and non-radiative (dm_{NR}/dt) recombination rates. Both models were subjected to a constant irradiation rate of $G = 1000\ cm^{-3}\ s^{-1}$ and a laboratory temperature of $T = 25\ ^{\circ}C$ during 3600 seconds.*

The decay of the trap I in both models is attributed to the fact that it is the closest trap to the Fermi level, and therefore the one with the lowest activation energy. This means that, even though the frequency factor is constant in the temperature independent model, the carriers will still be able to escape from this trap more easily than from the others. In the temperature dependent model we see that the decay of trap I is much more pronounced, as the thermal dynamics allow for a higher probability of detrapping. The other traps, on the other hand, remain mostly unnfafected due to their deeper energy levels, which result in significantly lower detrapping probabilities at the laboratory temperature. This contrast highlights the selective sensitivity of shallow traps to a certain thermal activation temperature, while deeper traps retain their occupancy over longer timescales. It also explains the need for a third stage of the process, where this temperature would be increased to allow the detrapping of all the excited electrons and holes and returning to the equilibrium state from the metastable state the material finds itself in after the relaxation phase.

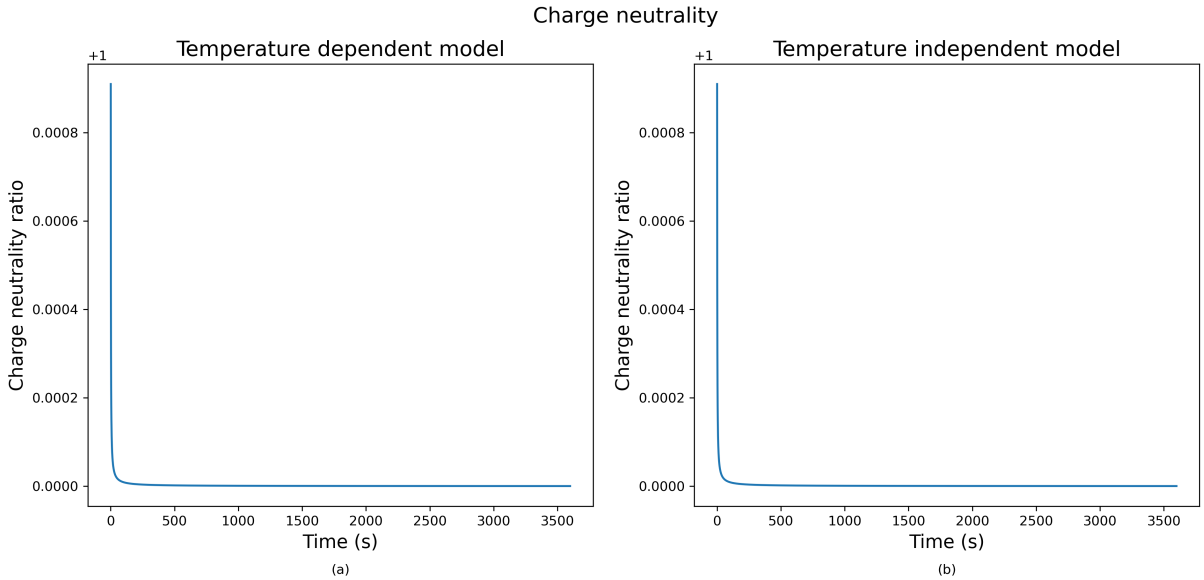

Figura 5.3: *Charge neutrality ratio for the LiF:Mg, Ti plotted against temperature during the irradiation phase for both models. (a) Temperature dependent model; (b) Temperature independent model. The plotted ratio corresponds to the total negative charge divided by the total positive charges in the system. Both simulations were performed under a constant generation rate of* $G = 1000\ cm^{-3}\ s^{-1}$ *and a laboratory temperature of* $T = 25\ ^{\circ}C$ *during 3600 seconds. The traps are labeled as follows: I (blue), II (orange), III (green), IV (red), V (purple), and s (brown).*

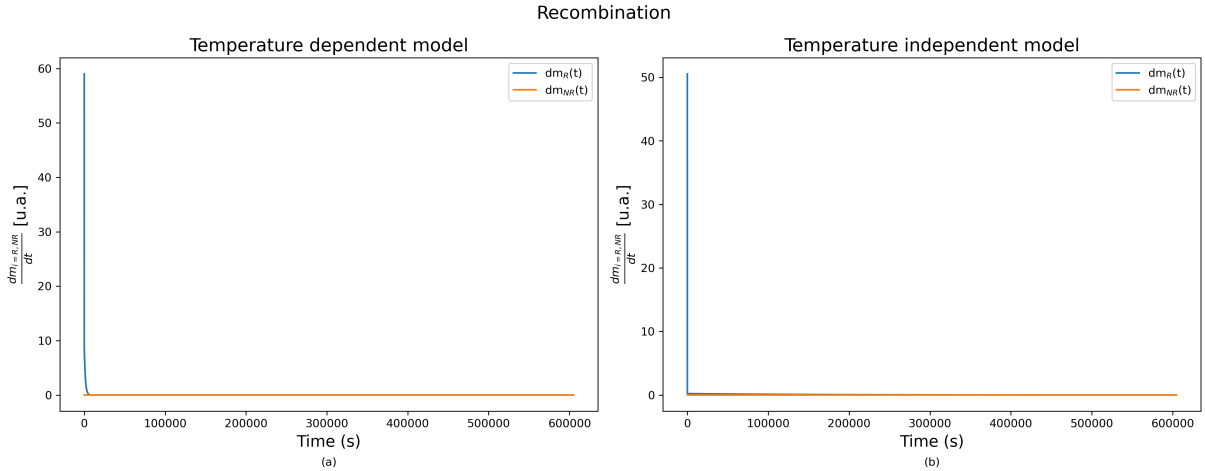

Figura 5.5: *Recombination rates for the LiF:Mg, Ti during the relaxation phase for both models. (a) Temperature dependent model; (b) Temperature independent model. The plotted quantities correspond to the radiative* (dm_R/dt) *and non-radiative* (dm_{NR}/dt) *recombination rates. Both models were subjected to a constant generation rate of* $G = 0\ cm^{-3}\ s^{-1}$ *and a laboratory temperature of* $T = 25\ ^{\circ}C$ *during 604,800 seconds.*

The next graph to analyze is the one showing the recombination rates during the relaxation stage, which can be seen in Figure 5.5. In this stage, the recombination rate $dm_{R(t)}$ exhibists a sharp decay in both models, consistent with the rapid depletion of free

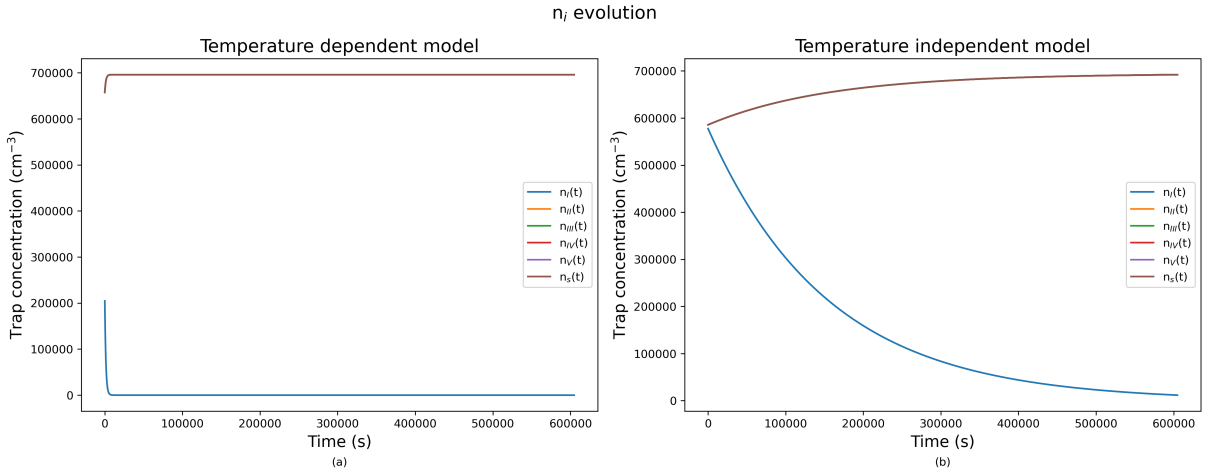

Figura 5.4: *Evolution of trap concentrations $n_i(t)$ plotted against time for the LiF:Mg, Ti during the relaxation phase for both models (a) Temperature dependent model; (b) Temperature independent model. Both were subjected to a constant generation rate of $G = 0\ cm^{-3}\ s^{-1}$ and a laboratory temperature of $T = 25\ ^{\circ}C$ during 604,800 seconds. The traps are labeled as follows: I (blue), II (orange), III (green), IV (red), V (purple), and s (brown).*

carriers following the irradiation stop. This behavior is driven by the thermal detrapping from the shallow traps –like the trap I we mentioned in the previous paragraph—, which quickly empties when stabilizing the laboratory temperature. Again, the nearly flat $dm_{NR}(t)$ in both cases suggests that non-radiative processes play a minimal role under these conditions.

Although the overal shape of the curves is similar, the temperature dependent model shows a more pronounced decay in the radiative recombination rate. This is due to the fact that, as we have seen in the previous section, the temperature dependent model allows for a higher occupation of traps, which leads to a higher probability of recombination. This is consistent with the fact that the temperature dependent model has a higher slope in the n_i evolution graph, as we saw in Figure 5.1.

The charge neutrality plots shown in Figure 5.6 confirm that the model preserves global charge conservation throughout the relaxation phase. Both the temperature independent and dependent model maintain a nearly perfect balance between positive and negative charges, with only a negligible deviation on the order of 10^{-6} at early times. The stability of these two plots supports the robustness of the simulations done for this phase, and reinforces the consistency of the relaxation dynamics.

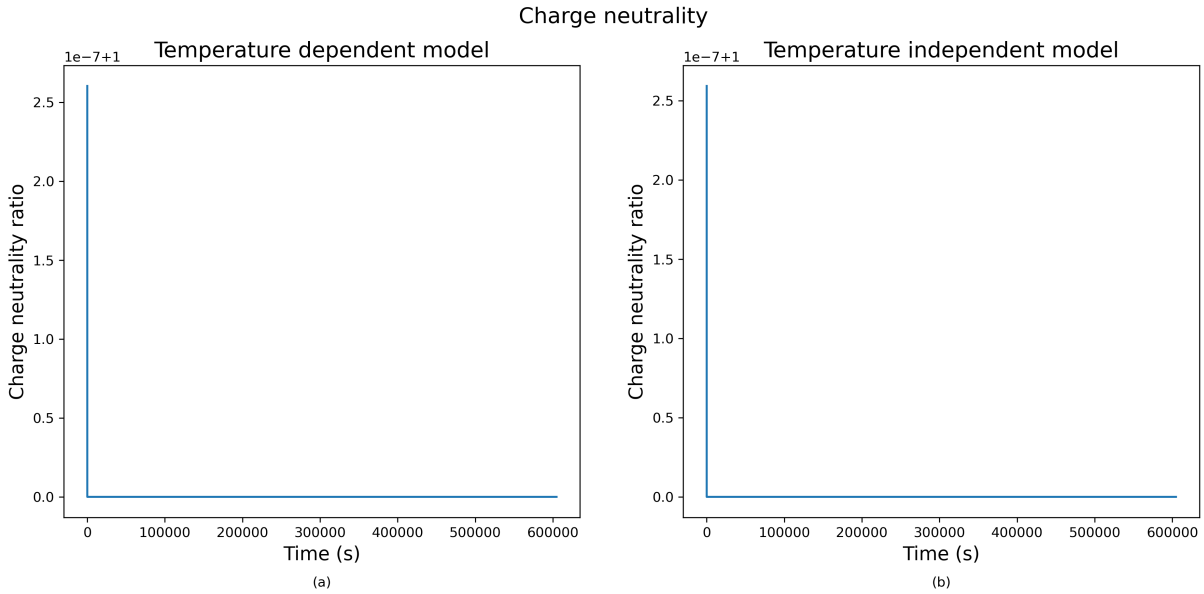

Figura 5.6: *Charge neutrality ratio for the LiF:Mg, Ti plotted against temperature during the relaxation phase for both models. (a) Temperature dependent model; (b) Temperature independent model. The plotted ratio corresponds to the total negative charge divided by the total positive charges in the system. Both simulations were performed under a constant generation rate of* $G = 0\ cm^{-3}\ s^{-1}$ *and a laboratory temperature of* $T = 25\ ^{\circ}C$ *during 604,800 seconds. The traps are labeled as follows: I (blue), II (orange), III (green), IV (red), V (purple), and s (brown).*

5.3. Heating

We can now move onto the last stage of the process, the *heating* stage. Here we will obtain the previously introduced TL glow curve, as one of the graphs we have been doing so far. The results obtained from the simulations in this section can be seen in Figures 5.7–5.9.

Before the TL glow curve, we must first analyze what is happening with the occupancy of the traps. Taking now the temperature in our X axis, we can see at a first glance in Figure 5.7, that both models show a similar behavior. As expected, the trap I is the first one to be emptied as it is the closest to the Fermi level. And as it has been seen, it is also here where we see the most significant difference between the two models. The starting point of trap I is notably lower in the tempreature dependent model, and can be attributed to thermal detrapping that we have already seen in the irradiation and relaxation stages, all of them due to the influence of the frequency factor. Because trap I we have seen to be shallow, even moderate temperature increase is sufficient to release the charged carriers. In the original model, we see that this trap withstands the temperature a little longer, and is not emptied until surpassing the first 100 °C.

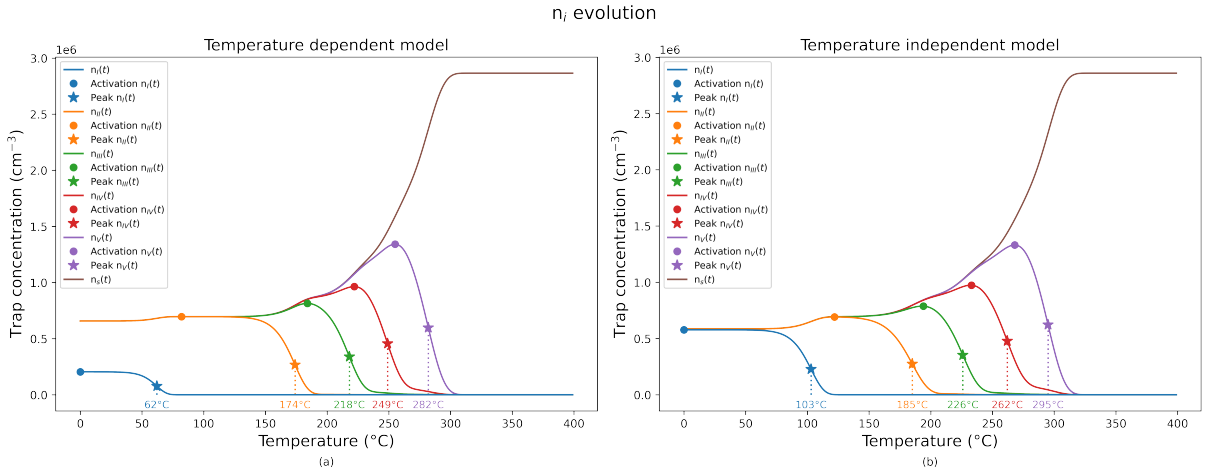

Figura 5.7: *Evolution of trap concentrations $n_i(t)$ for the LiF:Mg, Ti plotted against temperature during the heating phase for both models. (a) Temperature dependent model; (b) Temperature independent model. For each trap, both the activation temperature (filled circle) and peak temperature (star icon) are indicated. The peak temperature has a dotted line that reaches the X axis and indicates the specific value for each trap. The simulations were performed under a constant generation rate of $G = 0$ cm^{-3} s^{-1} and an increasing laboratory temperature from 0 °C to 400 °C during 400 seconds. The traps are labeled as follows: I (blue), II (orange), III (green), IV (red), V (purple), and s (brown).*

The evolution of traps II through V during the heating phase is mostly similar across both models. Each trap empties within its own temperature range, determined by its activation energy. After a certain *activation temperature* T_0 is reached, the traps will experience a sequencial release of carriers as temperature increases. On their way to emptying, they will go through a temperature at which the trap releases carriers at the highest rate. This temperature can be called *peak temperature* T_p, and it reflects the characteristic thermal energy required to efficiently empty that trap. It is directly related to the TL glow curve since the luminescence signal is proportional to the rate of carrier release from traps followed by radiative recombination (we remember this from equation 3.8), and therefore each peak observed in the TL glow curve corresponds to this same peak temperature T_p of a trap. Its position and shape provide valuable information about the trap's activation energy, so analyzing the evolution of trap occupancies and identifying their peak temperatures not only characterizes the thermal behavior of the system but also allows the interpretation of the TL glow curve based on the behavior of the traps.

In Figure 5.7, we see that trap s has neither of the characteristic temperatures, as it does not have a maximum. From this we can interpret that it does not follow the same behavior as the other traps because it does not empty at any temperature, but rather accumulates carriers when heated. This is consistent with its energetic position deep in the bandgap closer to the valence band, which implies that an electron captured in this state is highly unlikely, to the temperature range of this experiment, to be thermally re-excited. Such deep levels function as recombination centers rather than trapping states, and represent an irreversible endpoint for charge carriers released from shallower traps during the heating process [2]. For the traps I to V, it is clearly illustrated that the temperature peak depends on the range each trap has for their process of emptying.

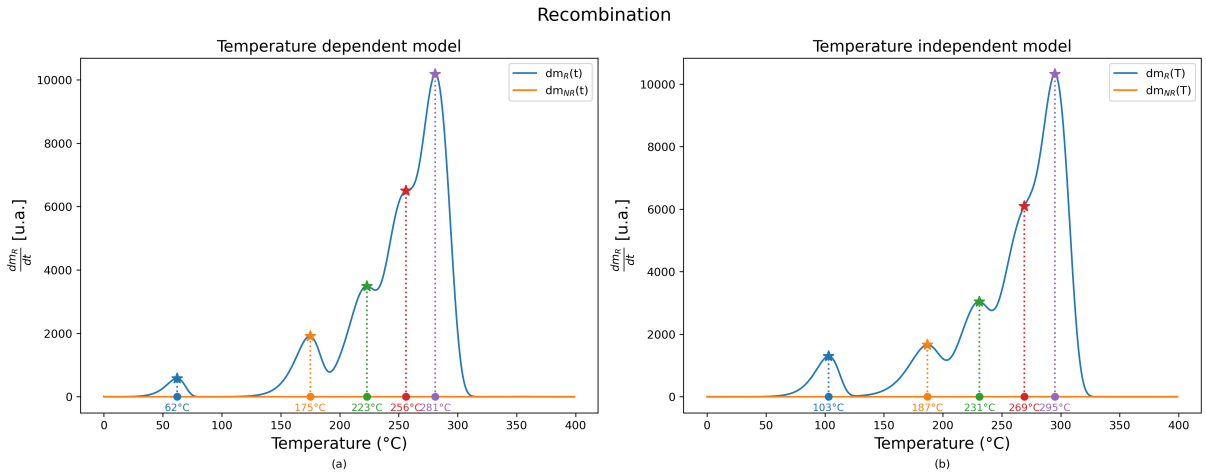

Figura 5.8: *Thermoluminescence (TL) glow curves for the LiF:Mg,Ti material plotted against temperature during the heating phase for both models. (a) Temperature dependent model; (b) Temperature independent model. The curves correspond to the radiative recombination rate dm_R/dt, showing the intensity of light emitted as trapped carriers recombine. For each visible peak, both the activation temperature (filled circle) and the peak temperature (star icon) are indicated. A vertical dotted line extends from each peak temperature to the X-axis, where the temperature value is labeled. The simulations were performed under a constant generation rate of $G = 0\ cm^{-3}\ s^{-1}$ and an increasing laboratory temperature from 0 °C to 400 °C during 400 seconds. The traps are labeled as follows: I (blue), II (orange), III (green), IV (red), V (purple), and s (brown).*

And now finally, we can obtain the TL glow curve from the simulations. In Figure 5.8 we can see that both models display the five distinct peaks of LiF:Mg, Ti, ranging from ∼ 60 °C to nearly ∼ 300 °C, and reflects the increasing activation energies and thermal stability of the traps involved, as the peaks that appear at higher temperatures have higher luminiscent response. Comparing both models reveals that the inclusion of temperature dependency in the frequency factor slightly shifts peak positions and modifies peak intensities, particularly in shallower traps. This suggest that the temperature depencency in the frequency factor influences the occupancy dynamics of lower-energy traps.

Furthermore, we can see that indeed the peak temperature values from 5.7 closely match those observed in the TL glow curve for both models. This strong agreement confirms that the temperature at which each trap empties coincides with the point of maximum luminescence intensity in the glow curve. Physically, this reinforces the interpretation that the TL glow peak directly reflects the maximum rate of carrier release from traps. The fact that this correspondence holds in both models despite their fundamental difference suggests that the thermal release of charge carriers is primarily governed by the intrinsic trap properties —such as activation energy, trap activation temperature and frequency factor— rather than by the specific thermal history prior to heating. This implies that the glow peak position is a robust indicator of trap characteristics, such as their activation mechanism, and luminiscent response.

qué más puedo decir?????

As a final note, we can check the validity of the model by looking at the charge neutrality condition, which can be seen in Figure 5.9. As we can see, both models satisfy the charge neutrality condition, as the total positive and negative charges are equal at all

times. This confirms that the model is consistent with the physical principles of charge conservation, and that the simulations have been done correctly.

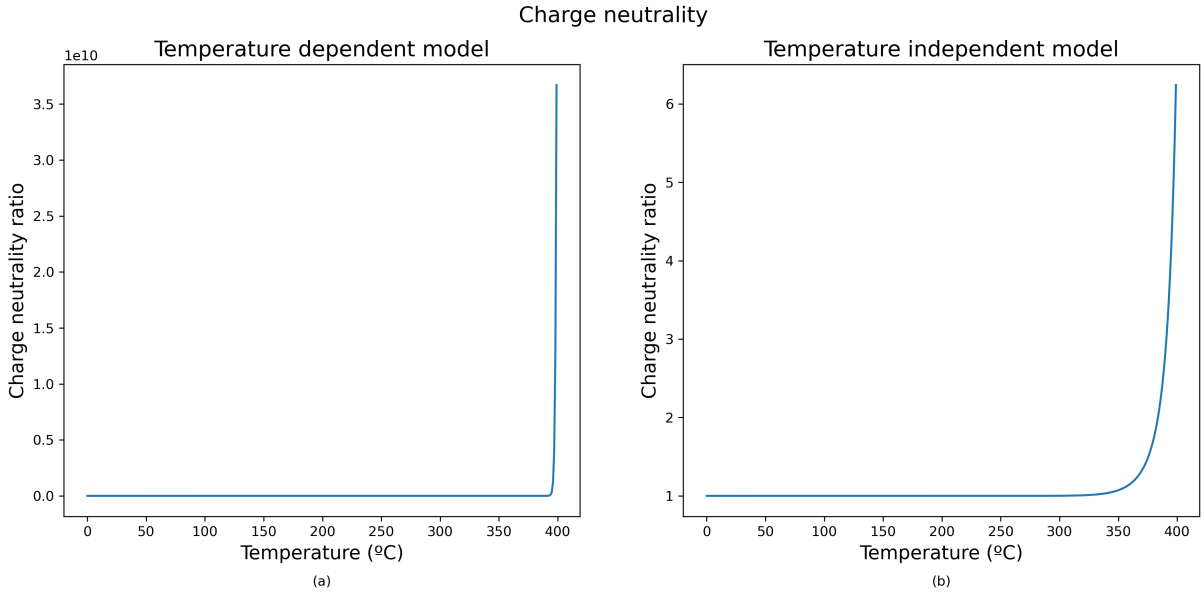

Figura 5.9: *Charge neutrality ratio for the LiF:Mg, Ti plotted against temperature during the heating phase for both models. (a) Temperature dependent model; (b) Temperature independent model. The plotted ratio corresponds to the total negative charge divided by the total positive charges in the system. Both simulations were performed under a constant generation rate of* $G = 0\ cm^{-3}\ s^{-1}$ *and an increasing laboratory temperature from 0 ˚C to 400 ˚C during 400 seconds. The traps are labeled as follows: I (blue), II (orange), III (green), IV (red), V (purple), and s (brown).*

Conclusiones

En este trabajo ...

Conclusions

In this work ...

Bibliografía

[1] Y. S. Horowitz, L. Oster, and H. Datz, The thermoluminescence dose response and other characteristics of the high-temperature TL in LiF:Mg,Ti (TLD-100), *Radiation Protection Dosimetry*, vol. 124, no. 2, pp. 191–205, Jun. 2007, doi: 10.1093/rpd/ncm241.

[2] McKeever, Stephen W. S. (2022). *A course in luminescence measurements and analyses for radiation dosimetry*. Wiley. ISBN 978-1-119-64689-1.

[3] J. J. Brey Abalo, *Mecánica estadística*, 1a ed., 6a reimp. Madrid: Universidad Nacional de Educación a Distancia, 2020. Colaboradores: J. de la Rubia Pacheco y J. de la Rubia Sánchez. ISBN: 978-84-362-4572-1.

[4] Halimi Mokhtar, Dahane Kadri, and Abdelmalek Mokeddem, "Simulation of the experimental thermal cleaning procedure in LiF:Mg,Ti and investigation of the origin of the first-order kinetics of its peaks,"*Modern Physics Letters B*, vol. 29, no. 35, p. 1550226, Dec. 2015, doi:10.1142/S0217984915502267.